AIR, WATER AND SOIL POLLUTION SCIENCE AND TECHNOLOGY

INDOOR AIR QUALITY

CONTROL, HEALTH IMPLICATIONS AND CHALLENGES

ROBERT M. RIDGWAY
EDITOR

NOVA

Air, Water and Soil Pollution Science and Technology

Air, Water and Soil Pollution Science and Technology

Urban Air Pollution and Avenue Trees: Benefits, Interactions and Future Prospects
Abhijit Sarkar, PhD (Editor), Sujit Das
2021. ISBN: 978-1-68507-175-2 (Hardcover)
2021. ISBN: 978-1-68507-474-6 (eBook)

Soil Conservation: Strategies, Management and Challenges
António Avelino Batista Vieira (Editor),
António José Bento Gonçalves (Editor)
2021. ISBN: 978-1-53619-513-2 (Hardcover)
2021. ISBN: 978-1-53619-600-9 (eBook)

Air Pollution: Effects and Dangers
Jorge Esteban Colman Lerner (Editor)
2021. ISBN: 978-1-53619-544-6 (Hardcover)
2021. ISBN: 978-1-53619-556-9 (eBook)

Air Quality Observation in the U.S.: Systems, Needs, and Standards
Malcolm Parisi (Editor)
2014. ISBN: 978-1-63117-154-3 (Hardcover)
2014. ISBN: 978-1-63117-164-2 (eBook)

Air Quality: Environmental Indicators, Monitoring and Health Implications
Arthur Hermans (Editor)
2013. ISBN: 978-1-62808-259-3 (Hardcover)
2013. ISBN: 978-1-62808-260-9 (eBook)

More information about this series can be found at
https://novapublishers.com/product-category/series/air-water-and-soil-pollution-science-and-technology/

Robert M. Ridgway
Editor

Indoor Air Quality

Control, Health Implications and Challenges

nova
science publishers
www.novapublishers.com

Library of Congress Cataloging-in-Publication Data

ISBN: 979-8-88697-181-1 (e-book)

Published by Nova Science Publishers, Inc. † New York

Contents

Chapter 1

Prediction of Heat Ventilation in Solar Air Heater Systems

Bdis Bakri[1], Ahmed Ketata[2], Slah Driss[2], Hani Benguesmia[3] and Zied Driss[2,*]

[1]Mechanical Engineering Department,
Faculty of Technology,
University of M'sila, M'sila, Algeria
[2]Laboratory of Electro-Mechanic Systems (LASEM),
National School of Engineers of Sfax (ENIS),
University of Sfax (US), Sfax, Tunisia
[3]LGE Laboratory,
Electrical Engineering Department,
Faculty of Technology,
University of M'sila, M'sila, Algeria

Abstract

In this chapter, we are interested on the design and the realization of a new solar air heater test bench to investigate the efficiency of the solar system. The considered test bench consists of two passages solar air heater separated by an absorber and powered by a fan working in a delivery mode. On the glass side, it is connected to the box prototype through a pipe. On this system, a glass is hanging on the front side and an absorber is inserted inside. The hot air flow is routed towards the box prototype. Two circular holes are located in the same face of the box prototype. The inlet hole allows the hot air supply. However, the outlet hole allows its escape into the ambient environment. Indeed, we have developed numerical simulations to study the turbulent flow in the

* Corresponding Author's Email: zied.driss@enis.tn.

In: Indoor Air Quality
Editor: Robert M. Ridgway
ISBN: 979-8-88697-134-7

considered test bench over the day. In these conditions, it has been observed a decrease in the flow and an appearance of the recalculation zones in the first passage. This phenomenon is more prominent during the transition of the flow to the second passage. However, the flow becomes uniform until the exit of the solar air heater. Via the pipe separating the solar air heater from the box prototype, a discharge area appears in the hole inlet and invaded the reverse wall. By comparing the local characteristics for the different instances, a similar appearance has been observed with a maximum value at t=12 hours. For the magnitude velocity, a small difference between the calculated values has been noted. However, this difference is more clear for the temperature distribution and the turbulent characteristics. For the energy efficiency, it presents very low values at the beginning of the day. With the increase of the temperature through the day, there is a gradual increase of the energy efficiency until t=12 hours, with a value equal to η= 31,8%. This technology will be very useful since it can provide sustainable energy and substitute the expensive traditional technologies.

Keywords: solar air heater, sustainable energy, ventilation, aerodynamic structure, CFD

1. Introduction

The use of the solar energy in heat ventilation is widely applied, such as hospitals, residential and commercial buildings. The objective is to minimize energy consumption with the use of renewable energy [1-21]. In this context, Yang et al. [22] designed a solar air heater with offset strip fins optimized by numerical modeling. Then, a series of experiments based on ASHRAE Standard 93-2003 was conducted to test the detailed thermal performance of the heater in the light of time constant, thermal efficiency, incident angle modifier and the synthetically resistance coefficient. Altaa et al. [23] compared three different types of designed flat-plate solar air heaters, two having fins and the other without fins. One of the heater with a fin had single glass cover and the others had double glass covers. Based on the energy output rates, heater with double glass covers and fins is more effective and the difference between the input and output air temperature is higher than of the others. Zukowski [24] presented a novel construction of a forced air solar heater based on a confined single slot jet of air impinging on the flat surface of an absorber plate. The results of experimental research showed that the efficiency of energy conversion ranges from 66% up to 90%. El-Sebaii et al.

[25] developed a comparison between the measured outlet temperatures of flowing air, temperature of the absorber plate and output power of the double pass-finned and v-corrugated plate solar air heaters. The results confirmed that the double pass v-corrugated plate solar air heater is 9.3–11.9% more efficient compared to the double pass-finned plate solar air heater. Wazed et al. [26] confirmed that the fabricated solar air heater is working efficiently. Esen [27] presented an experimental energy and exergy analysis for a novel flat plate SAH with several obstacles and without obstacles. The results confirm that the optimal value of efficiency is a middle level of absorbing plate in flow channel duct for all operating conditions. The double-flow collector supplied with obstacles appears significantly better than that without obstacles. Based on these previous studies, it is clear that the use of the SAH system with the double pass is more efficient. For this, we focused our attention on the study of a new SAH system with double pass designed and realized in our laboratory. In the present chapter, we are interested on the prediction of the heat ventilation and the experimental validation with the considered test bench.

2. Solar Air Heater System

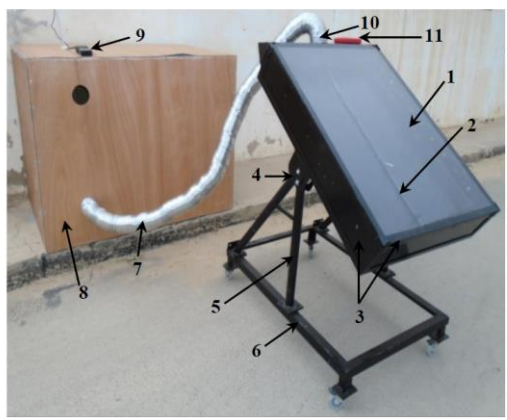

N°	Designation
1	Glass cover
2	Absorber plate
3	Insulation
4	Clevis
5	Mounting brackets
6	Mobile base
7	Duct
8	Box prototype
9	Anemometer
10	Fan
11	Multi meter

Figure 1. Solar air heater test bench.

Figure 1 presents the new solar air heater test bench designed and realized in our LASEM laboratory to investigate the efficiency of the solar system. The considered system consists of a two passages solar air heater separated by an absorber and powered by a fan working in a delivery mode and placed in the

inlet, side the insulation. On the glass side, it is connected to the box prototype through a pipe.

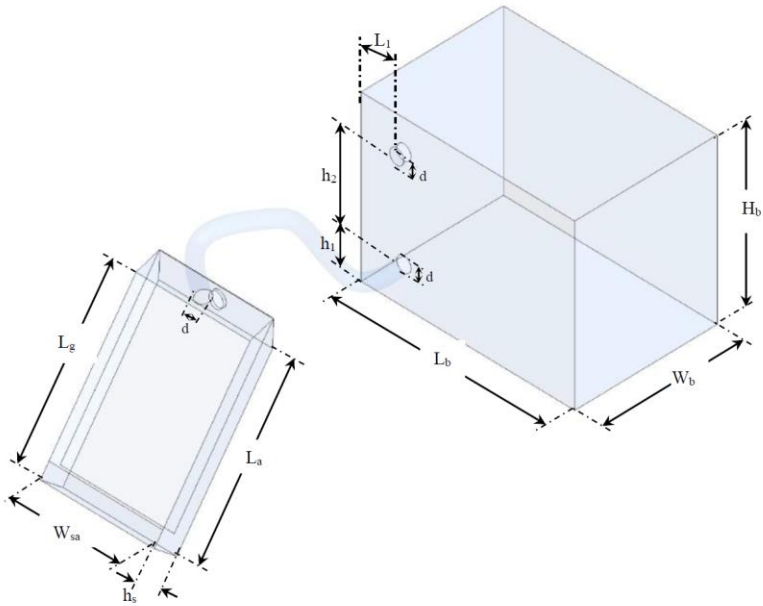

Parameters	Value(mm)
Length of the box prototype L_b	1500
Height of the box prototype H_b	1100
Width of the box prototype W_b	1000
Longitude of the holes L_1	300
Length of the absorber L_a	1086
Length of the glass L_g	1000
Width of the solar air heater W_s	778
Height of the solar air heater h_s	194
Altitude of the holes inlet h_1	250
Distance between of the two holes h_2	900
Diameters of the holes d	100

Figure 2. Geometrical arrangements.

The geometrical arrangements of the computational domain are presented in Figure 2, which is composed of two domains separated by a circular pipe with a diameter d=100 mm. The first one is the solar air heater with a height h_s=194 mm and a width W_s=778 mm. On this system, a glass is hanging on the front side with a length L_g=1000 mm and an absorber is inserted inside

with a length L_a=1086 mm. The hot air flow is routed towards the box prototype with a length L_b=1500 mm, a height H_b=1100 mm and a width W_b=1000 mm. Two circular holes, with a distance h_2=900 mm, are located in the same face of the box prototype. The inlet holes, placed in the altitude h_1=250 mm and a longitude L_1=300 mm, allows the hot air supply. However, the outlet hole allows its escape into the ambient environment.

3. Numerical Model

3.1. Boundary Conditions

A boundary condition is required anywhere fluid enters or exits the system and can be set as a pressure inlet, mass flow inlet, interior, internal or interface. General interpretation was given on the basis of numerical simulation of the solar air heater. A physical model was simulated using ANSYS Fluent 17.0, based on the geometrical dimensions of the solar air heater. The boundary conditions are illustrated in Figure 3. Wall boundary was applied for the solar air heater with heat flux of value equal zero to obtain the adiabatic wall. Wall boundary was used for the absorber and the mirror and convective heat transfer option was applied for different parts of the device such as glass and absorber. For the inlet velocity, it has been taken a magnitude velocity equal to V=3 $m.s^{-1}$. For the pressure outlet, a value of p=101325 Pa is set. This means that at this opening the fluid exits the model to an area of static atmospheric pressure condition.

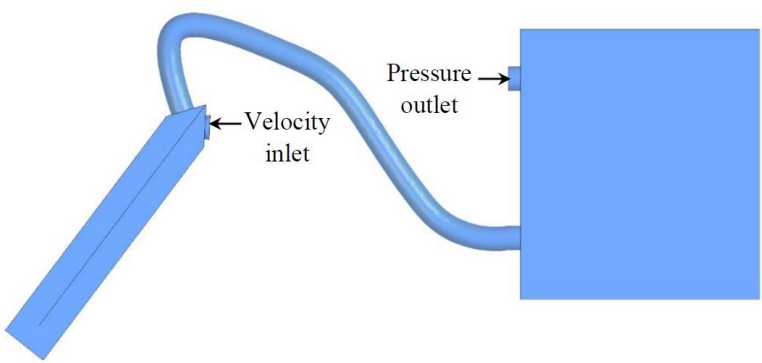

Figure 3. Boundary conditions.

3.2. Meshing

The automatically generated mesh is usually appropriate and intricate problems with thin and small meshing. Geometrical and physical features can result in extremely high number of cells, for which the computer memory is too small. “Meshing” options allow us to manually adjust the computational mesh to solve problems features and to resolve them better. In this application, we have adopted the refined model consisting of a maximum number of cells equal to N=1578369 cells that gives the lower numerical diffusion inside the solar air heater with an unstructured and tetrahedral meshing as presented in Figure 4.

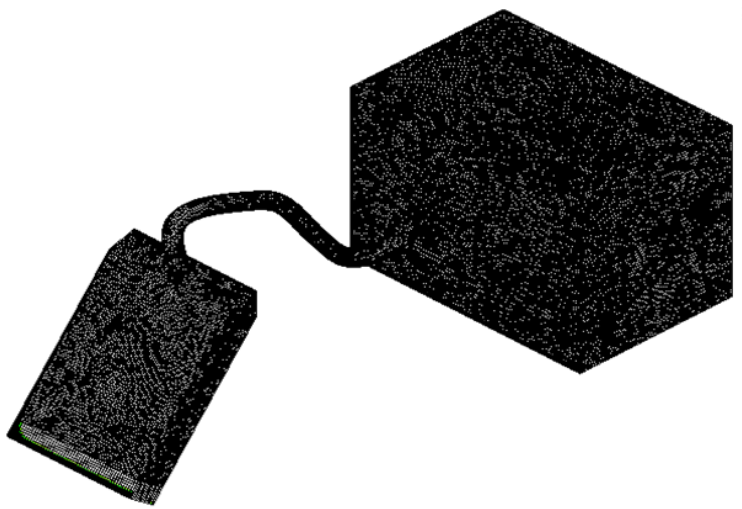

Figure 4. Meshing of the computational domain.

4. Results and Discussion

The distribution of the velocity fields, the temperature, the Do irradiation, the total pressure, the turbulent kinetic energy, the turbulence eddy frequency and the turbulent viscosity are presented in this section. In our case, the Reynolds number is evaluated to be equal to Re=20000. Particularly, we have considered different longitudinal and transverse planes for the first and second passages of the solar air heater supplying the box prototype, as presented in Figure 5.

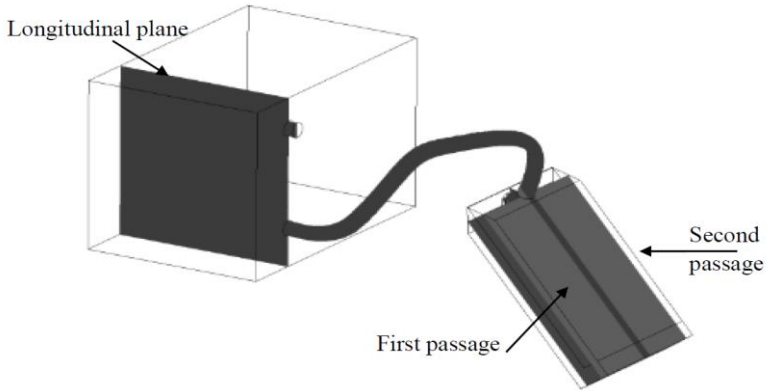

Figure 5. Visualization planes.

4.1. Velocity Fields

Figures 6, 7 and 8 show the velocity fields distribution in the different longitudinal and transverse planes for the first and second passages of the solar air heater supplying the box prototype at t=10 hours, t=12 hours, t=14 hours and t=16 hours. According to these results, it is clear that the velocity fields present the same distribution at the different considered instances. For example, at t=12 hours the inlet velocity is governed by the boundary condition defined by V=3 $m.s^{-1}$. In the first passage, a decrease in the flow has been observed and a recirculation zone is created. This phenomenon is more prominent during the transition of the flow to the second passage. In this side, the flow becomes uniform until the exit of the solar air heater.

Indeed, the velocity reaches a very important value equal to V=5 $m.s^{-1}$. Via the pipe separating the solar air heater from the box prototype, a discharge area appears in the hole inlet and invaded the reverse wall. At this level, the velocity changes his direction and two axial flows have been observed. The first ascending flow is responsible on the recirculation zone appeared in the wholes area of the box prototype. This movement continues until the exit of the air flow through the hole outlet and reaches the maximum value equal to V=4 $m.s^{-1}$. The second descending flow is due to the dead zone appeared in the down area. Globally, the averaged velocity value is about V=1.5 $m.s^{-1}$ in the discharge area. Elsewhere, the averaged velocity presents a very low value. By comparing the velocity fields for the different instances, it is clear that the maximum value of the average velocity is obtained at t=12 hours. For the other

instances, the magnitude velocity decreases and the minimum values are obtained at t=16 hours.

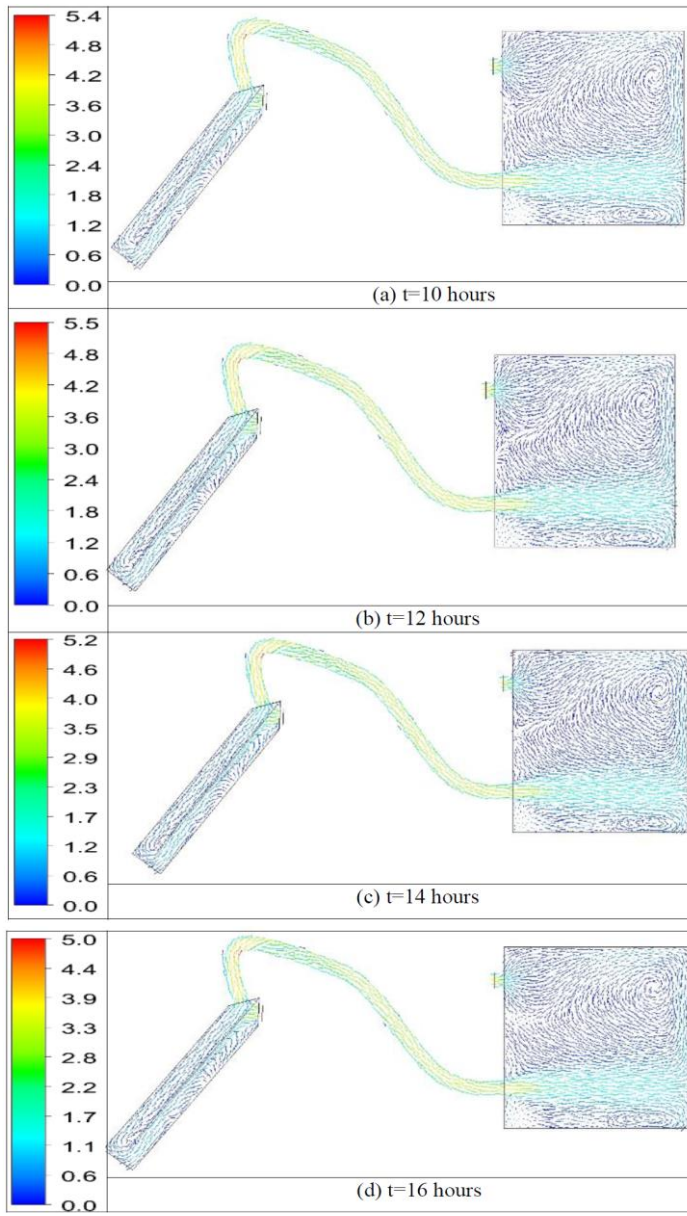

Figure 6. Distribution of the velocity fields in the longitudinal plane.

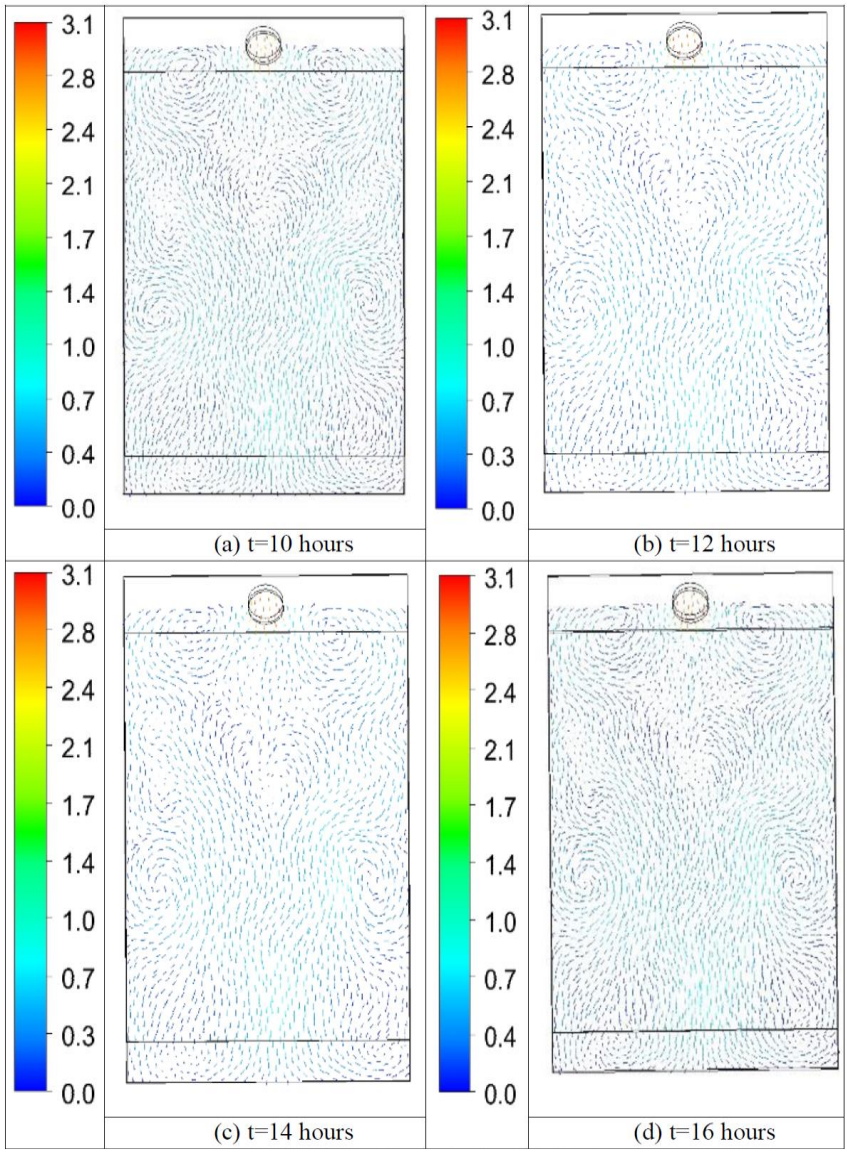

Figure 7. Distribution of the velocity field in the first passage.

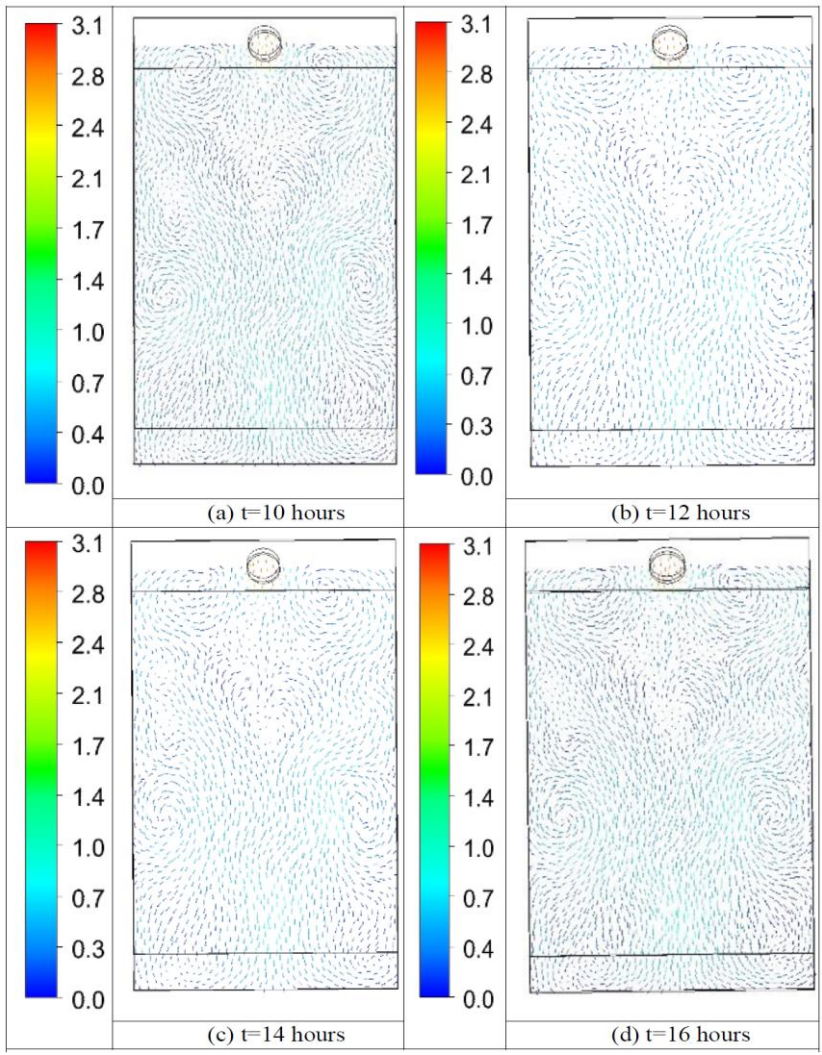

Figure 8. Distribution of the velocity field in the second passage.

4.2. Temperature

Figures 9, 10 and 11 show the distribution of the temperature in the different longitudinal and transverse planes for the first and second passages of the solar air heater supplying the box prototype at t=10 hours, t=12 hours, t=14 hours

and t=16 hours. According to these results, it is clear that the temperature presents the same distribution at the different considered instances. For example, at t=12 hours it has been noted that the inlet temperature is governed by the boundary condition defined by T=308 K. This value increases immensely and reaches an average value equal to T=338 K in the first passage and T=347 K in the second passage. This fact can be explained by the air flow incoming at ambient temperature and flowing the channel between the absorber plane and the insulation, which starts warming up by the convection with the absorber. In the second passage, the temperature of the air flow is more important since the flowing between the glass and the absorber is affected by the solar radiations. Thereby, the box prototype is powered by a continuous air heater characterized by the maximum temperature value equal to T=349 K. By comparing the temperature for the different instances, it is clear that the maximum value of the temperature is obtained at t=12 hours. For the other instances, the temperature decreases and the minimum values are obtained at t=16 hours. At this instance, the maximum value of the temperature is equal to T=340 K.

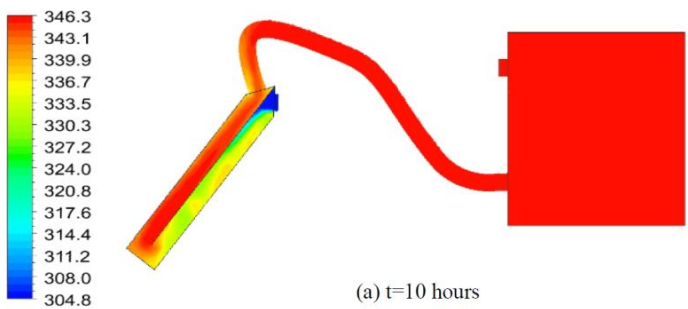

(a) t=10 hours

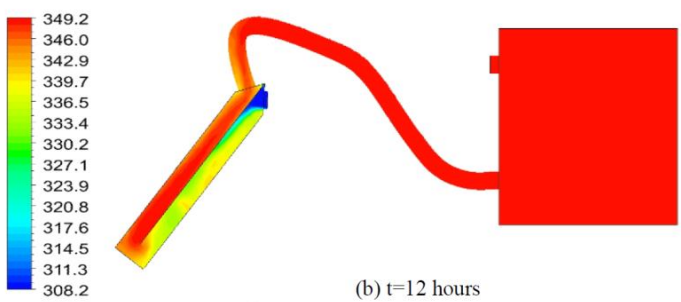

(b) t=12 hours

Figure 9. (Continued onto next page).

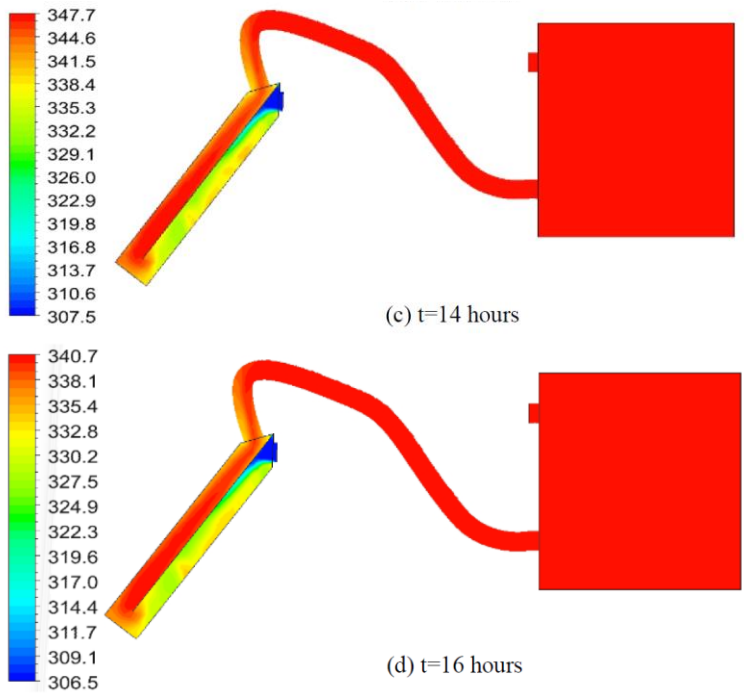

Figure 9. Distribution of the temperature in the longitudinal plane.

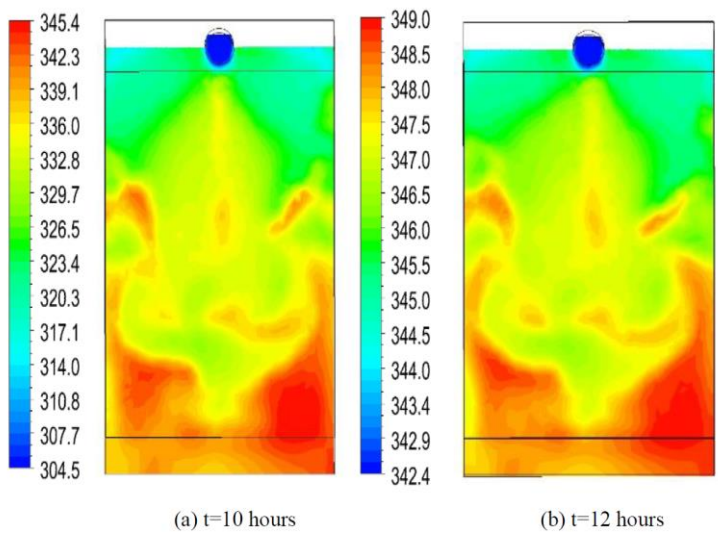

Figure 10. (Continued onto next page).

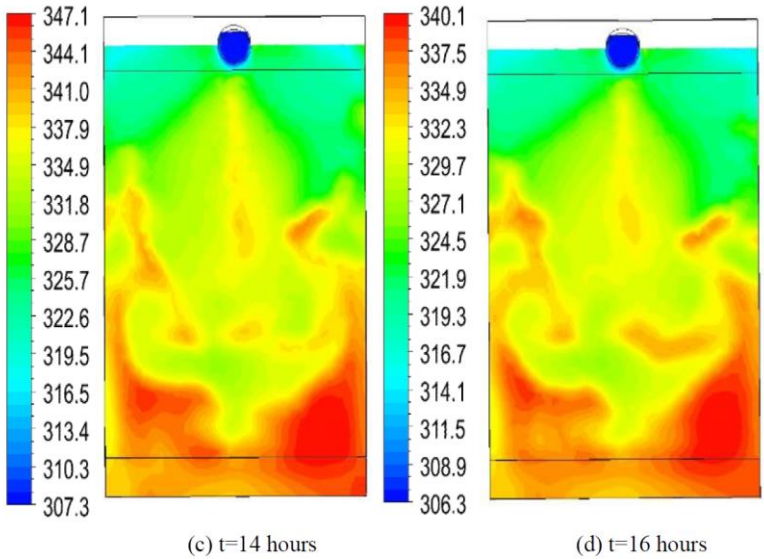

Figure 10. Distribution of the temperature in the first passage.

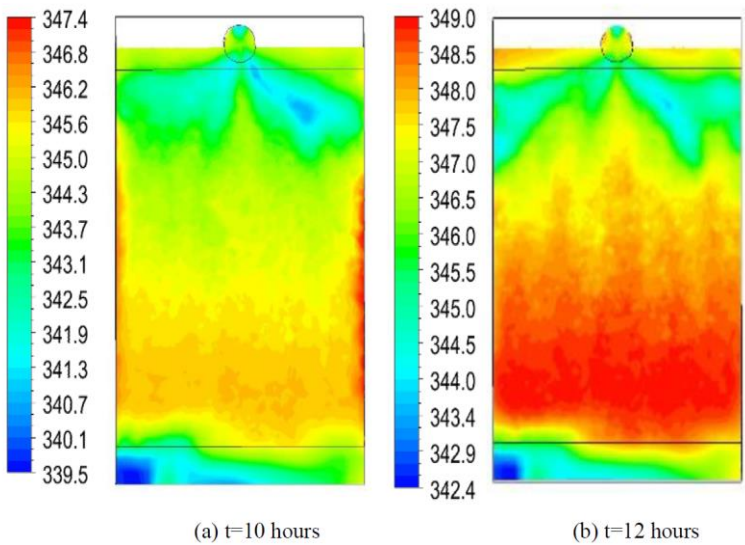

Figure 11. (Continued onto next page).

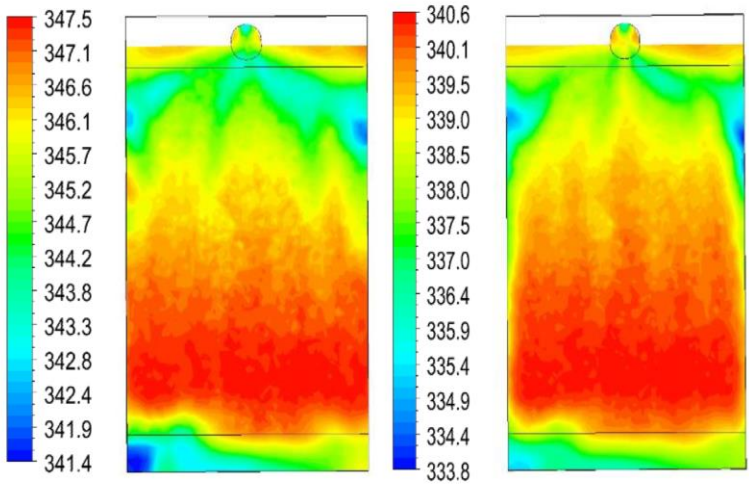

Figure 11. Distribution of the temperature in the second passage.

4.3. Distribution of the Do Irradiation

Figures 12, 13 and 14 show the distribution of the Do irradiation in the different longitudinal and transverse planes for the first and second passages of the solar air heater supplying the box prototype at t=10 hours, t=12 hours, t=14 hours and t=16 hours. From these results, it is clear that the Do irradiation presents the same distribution at the different considered instances. For example, at t=12 hours it has been observed that the Do irradiation presents a low value equal to I=2500 $W.m^{-2}$ in the inlet of the solar air heater. This value increases immensely and reaches the maximum value I=3375 $W.m^{-2}$ near the absorber in the second mid-plane of the first passage of the solar air heater. In the second passage a gradual decrease of the Do irradiation has been observed with an average value equal to I=3200 $W.m^{-2}$. The minimum value of the Do irradiation equal to I=2650 $W.m^{-2}$ has been observed in the second mid-plane of the second passage of the solar air heater. From the inlet of the pipe, attached to the solar air heater, the Do irradiation reaches the maximum value equal to I=3375 $W.m^{-2}$ in all the field of the box prototype. By comparing the Do irradiation for the different instances, it is clear that the maximum value of the Do irradiation is obtained at t=12 hours. For the other instances, the Do irradiation decreases and the minimum values are obtained at t=16 hours. At

this instance, the maximum value of the Do irradiation is equal to I=3060 $W.m^{-2}$.

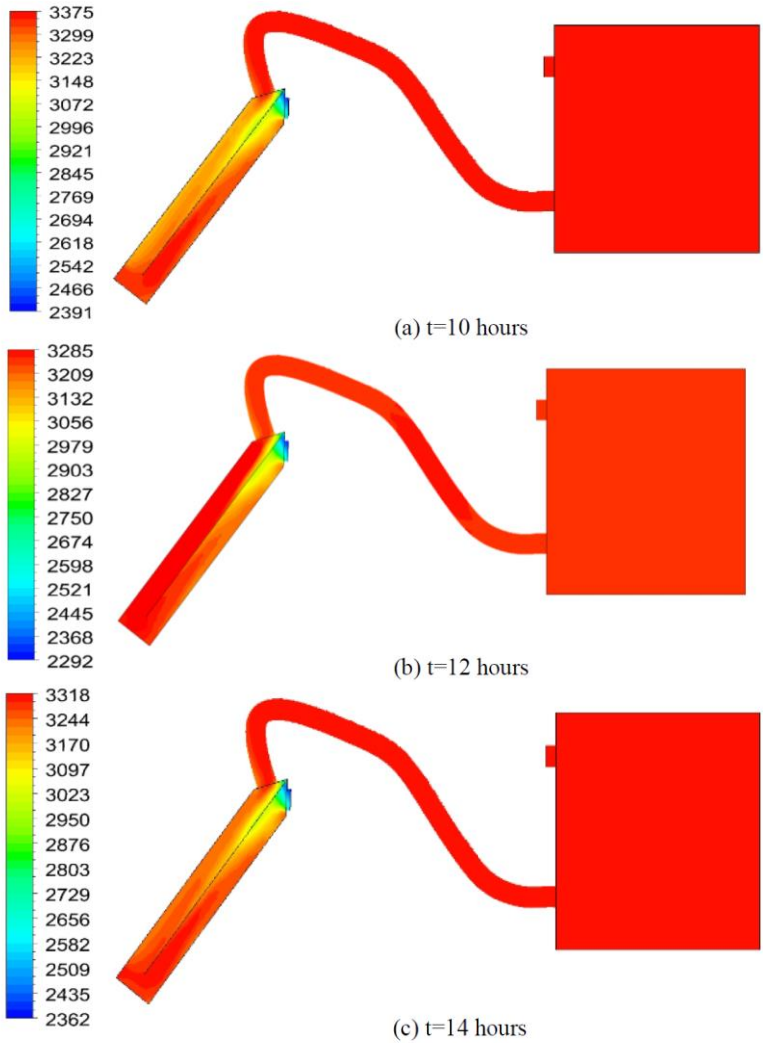

Figure 12. (Continued onto next page).

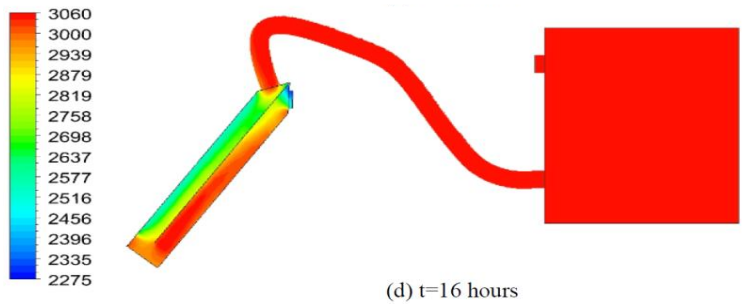

Figure 12. Distribution of the Do Irradiation in the longitudinal plane.

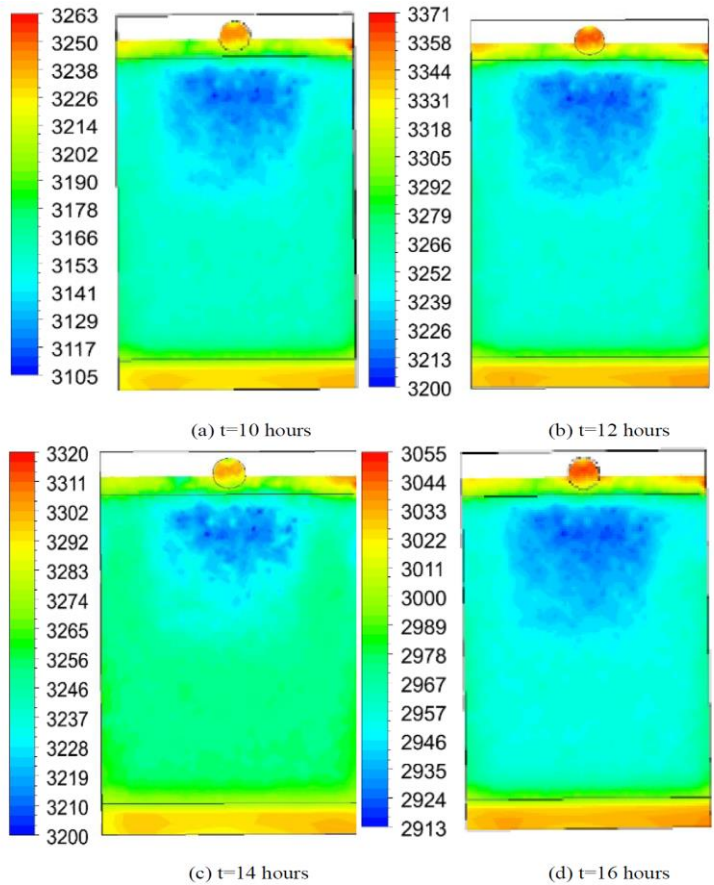

Figure 13. Distribution of the Do Irradiation in the first passage.

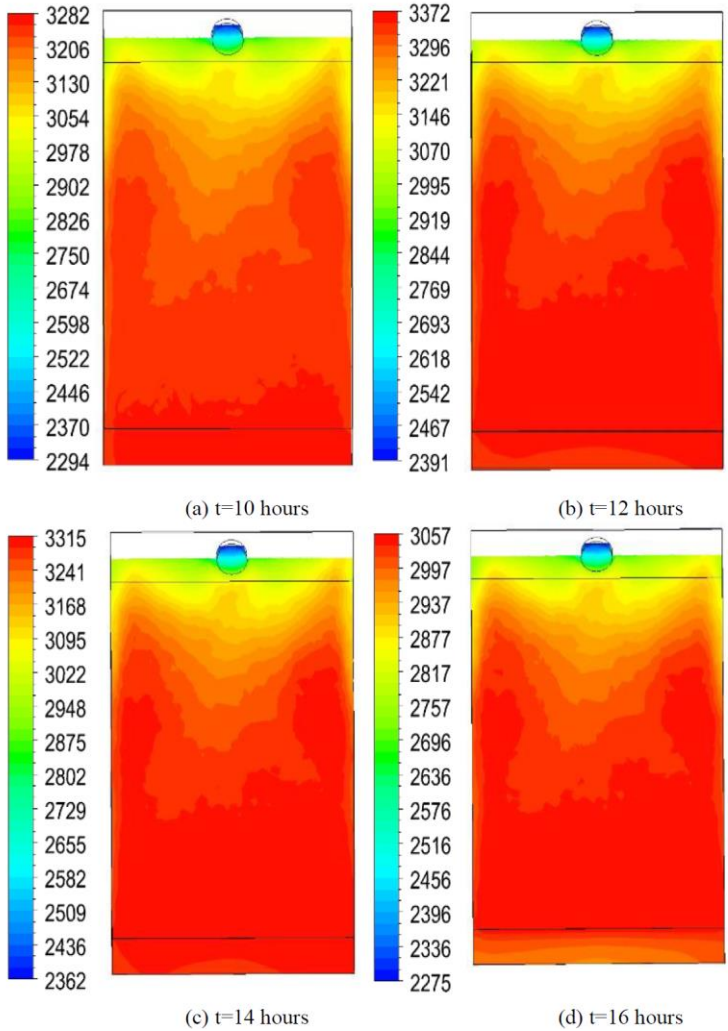

Figure 14. Distribution of the Do Irradiation in the second passage.

4.4. Total Pressure

Figures 15, 16 and 17 show the distribution of the total pressure in the different longitudinal and transverse planes for the first and second passages of the solar air heater supplying the box prototype at t=10 hours, t=12 hours, t=14 hours and t=16 hours. From these results, it is clear that the total pressure presents

the same distribution at the different considered instances. For example, at t=12 hours a compression zone characteristic of the maximum value of the total pressure has been observed in the collector inlet. Then, the total pressure decreases and presents a stabilized value, equal to p=101365 Pa, in the remaining domain of the two passages of the solar air heater. At the exit of the second passage, the total pressure continues decreasing along the pipe and reaches a value equal to p=101347 Pa in the inlet of the box prototype. Through the air advancement, the total pressure decreases quietly in the expulsion area, produced from the hole inlet and invaded until the reverse wall. This fact can be explained by the recirculation zone appeared in the wholes area of the box prototype. In the hole outlet, a depression zone characteristic of the minimum value, equal to p=101327 Pa, has been observed. By comparing the total pressure for the different instances, it is clear that the maximum value of the total pressure is obtained at t=12 hours and it is equal to p=101372 Pa. For the other instances, the total pressure decreases and the minimum values are obtained at t=16 hours. At this instance, the maximum value of the total pressure is equal to p=101351 Pa.

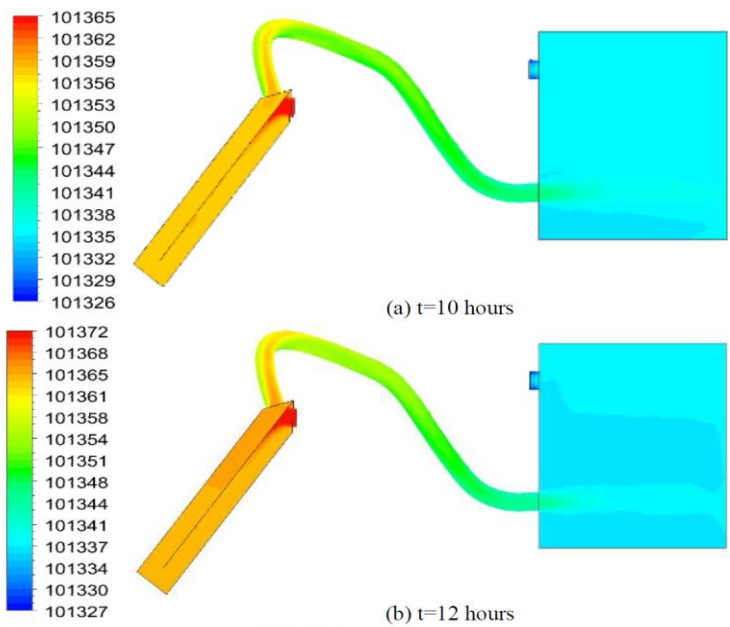

Figure 15. (Continued onto next page).

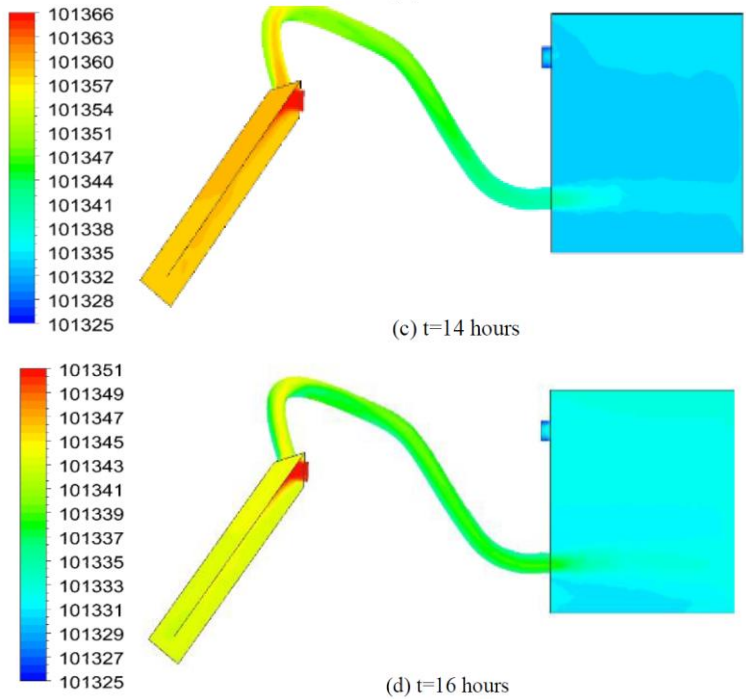

Figure 15. Distribution of the total pressure in the longitudinal plane.

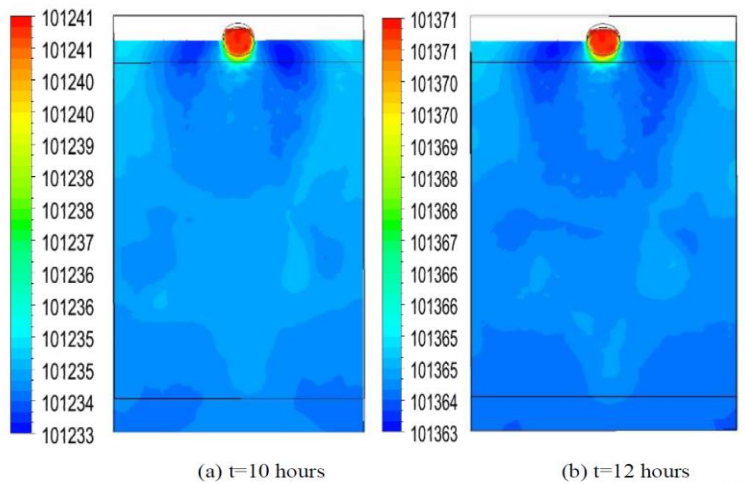

Figure 16. (Continued onto next page).

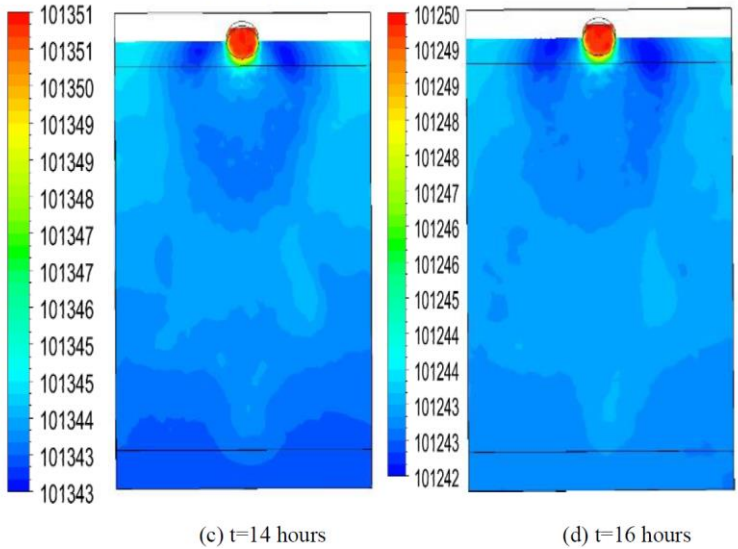

Figure 16. Distribution of the total pressure in the first passage.

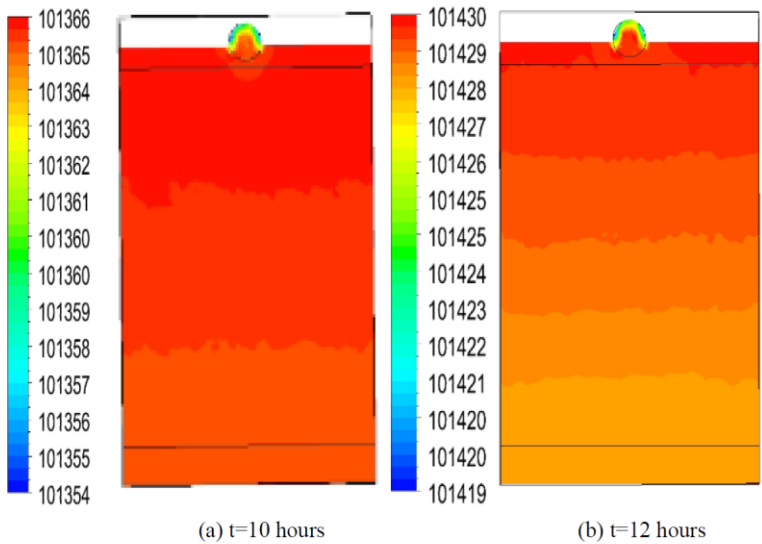

Figure 17. (Continued onto next page).

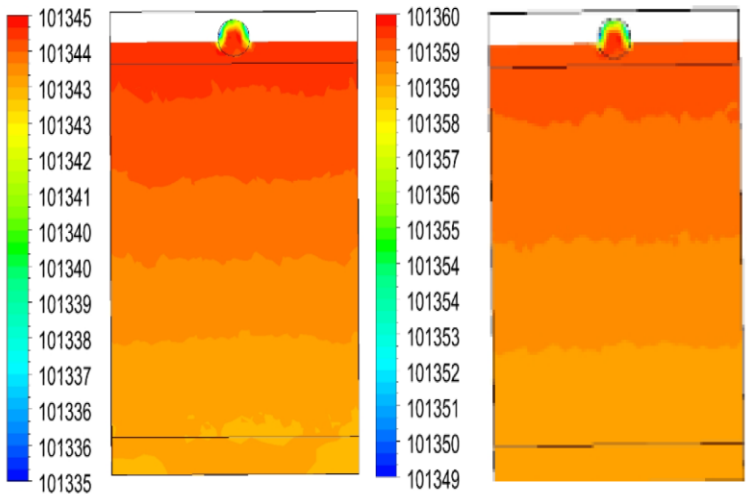

Figure 17. Distribution of the total pressure in the second passage.

4.5. Turbulent Kinetic Energy

Figures 18, 19 and 20 show the distribution of the turbulent kinetic energy in the different longitudinal and transverse planes for the first and second passages of the solar air heater supplying the box prototype at t=10 hours, t=12 hours, t=14 hours and t=16 hours. According to these results, it is clear that the turbulent kinetic energy presents the same distribution at the different considered instances. For example, at t=12 hours a wake zone characteristic of the maximum value of the turbulent kinetic energy has been observed around the collector inlet of the solar air heater. This wake is expanded in the first passage near the absorber side and until the mid-plane. In these conditions, the maximum value of the turbulent kinetic energy is equal to $k=0.98\ m^2.s^{-2}$. Away from this area, the turbulent kinetic energy presents a very weak value excepting the lower leading edge of the absorber, where the turbulent kinetic energy is equal to $k=0.09\ m^2.s^{-2}$. At the exit of the second passage, a second wake zone characteristic of the maximum value of the turbulent kinetic energy appears and extends along the first part of the pipe connecting the solar air heater with the box prototype. After the decrease of the turbulent kinetic energy in the second part of the pipe, an expulsion area appears in the hole inlet of the box prototype and invaded in the discharge area

until the reverse wall. This fact can be explained by the recirculation zone appeared in the whole area of the box prototype. Indeed, a slightly decrease of the turbulent kinetic energy has been observed outside this area. However, in the outlet of the box prototype, a wake zone characteristic of the maximum value of the turbulent kinetic energy has been appeared. By comparing the turbulent kinetic energy for the different instances, it is clear that the maximum value of the turbulent kinetic energy is obtained at t=12 hours and it is equal to k=1.157 $m^2.s^{-2}$. For the other instances, the turbulent kinetic energy decreases and the minimum values are obtained at t=16 hours. At this instance, the maximum value of the turbulent kinetic energy is equal to k=1.111 $m^2.s^{-2}$.

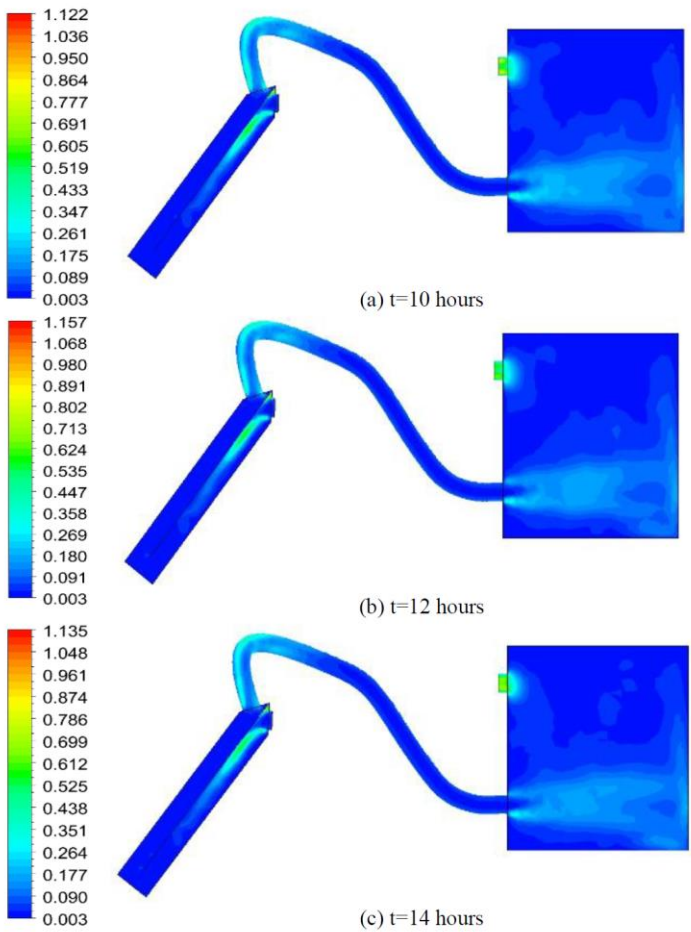

Figure 18. (Continued onto next page).

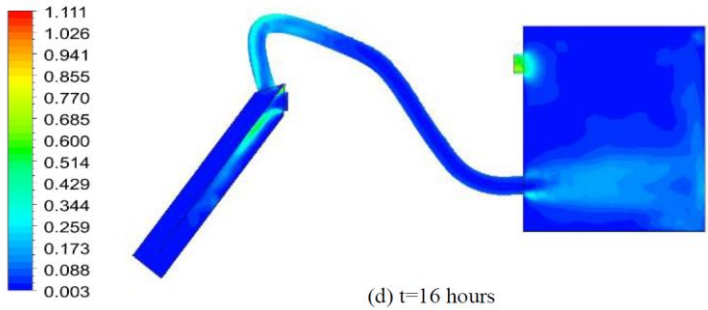

Figure 18. Distribution of the turbulent kinetic energy in the longitudinal plane.

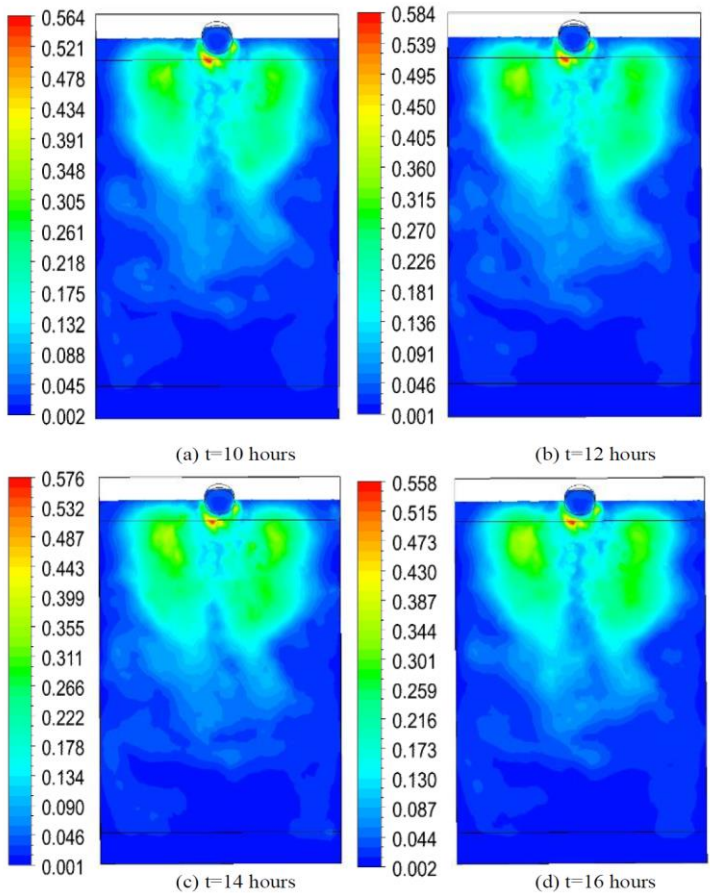

Figure 19. Distribution of the turbulent kinetic energy in the first passage.

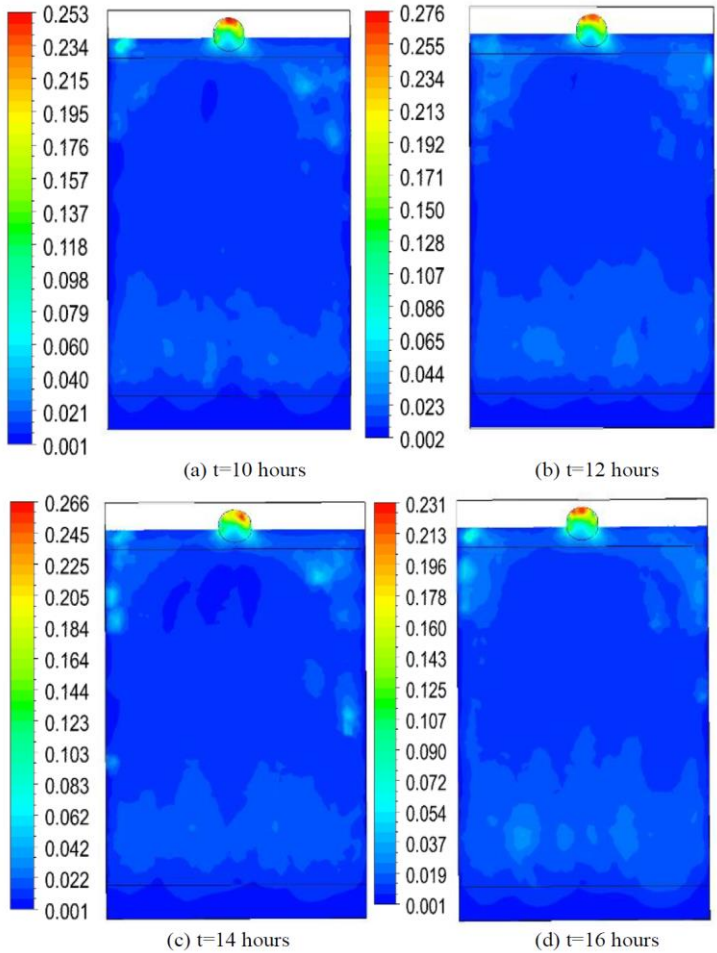

Figure 20. Distribution of the turbulent kinetic energy in the second passage.

4.6. Turbulent Eddy Frequency

Figures 21, 22 and 23 show the distribution of the turbulent eddy frequency in the different longitudinal and transverse planes for the first and second passages of the solar air heater supplying the box prototype at t=10 hours, t=12 hours, t=14 hours and t=16 hours. According to these results, it is clear that the turbulent eddy frequency presents the same distribution at the different considered instances. For example, at t=12 hours, a wake zone characteristic

of the maximum value of the turbulent eddy frequency has been created from the collector inlet of the solar air heater, with a moderate value of the turbulent eddy frequency equal to ω=300 s^{-1}. This wake is expanded in the first passage near the absorber side and until the mid-plane. In these conditions, the maximum value of the turbulente eddy frequency is equal to ω=500 s^{-1}. Away from this area, the turbulent eddy frequency decreases and reaches a low value equal to ω=40 s^{-1} at the bottom of the collector where the insulator is localized. Through the second passage and away from the glass and the absorber, the turbulent eddy frequency continues the decreases even more and reaches a null value in the upper half plane. In the pipe connecting the solar air heater with the box prototype, the turbulent eddy frequency increases and reaches a maximum value equal to ω=500 s^{-1}. By comparing the turbulent eddy frequency for the different instances, it is clear that we found the same results. In all these cases, the maximum value of the frequency is equal to ω=308 s^{-1}.

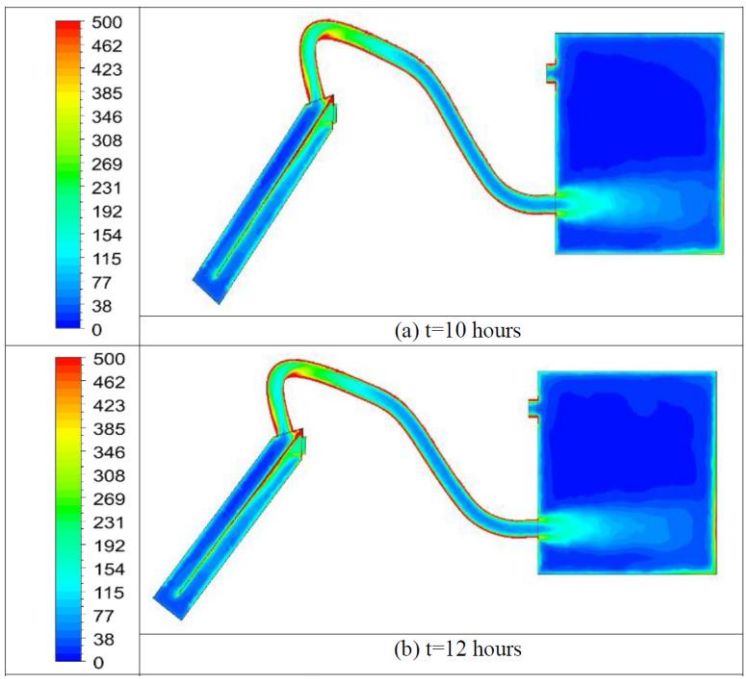

Figure 21. (Continued onto next page).

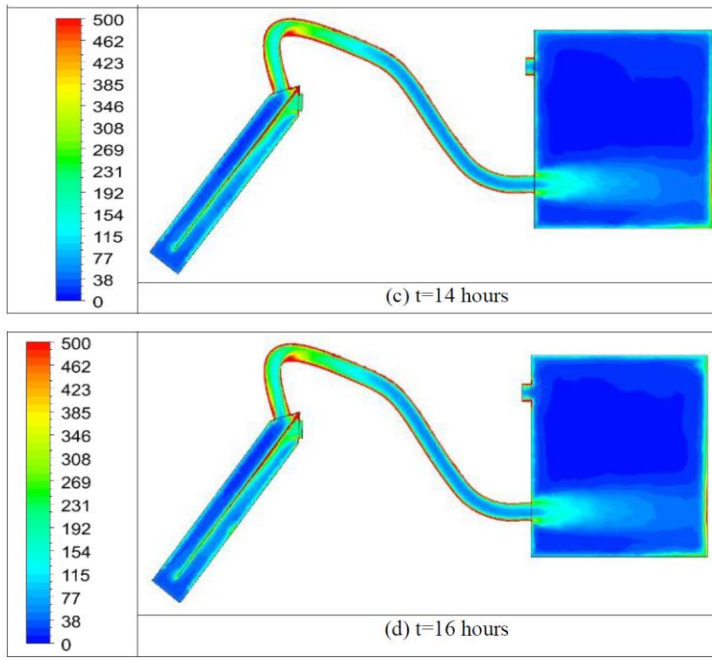

Figure 21. Distribution of the Turbulence Eddy Frequency in the longitudinal plane.

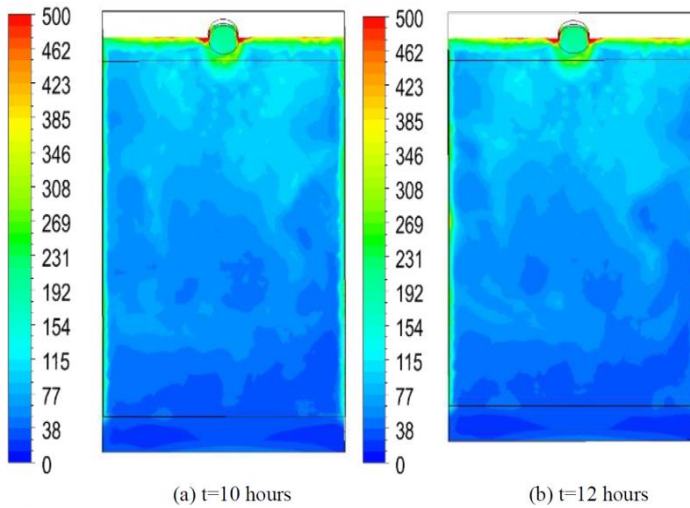

Figure 22. (Continued onto next page).

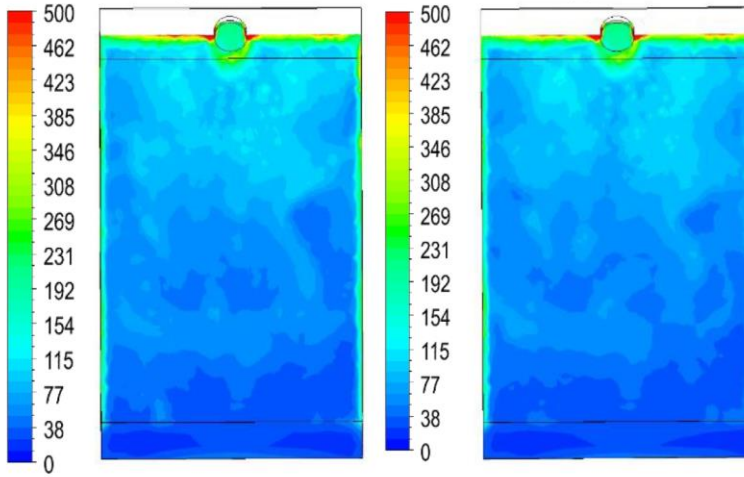

Figure 22. Distribution of the turbulent eddy frequency in the first passage.

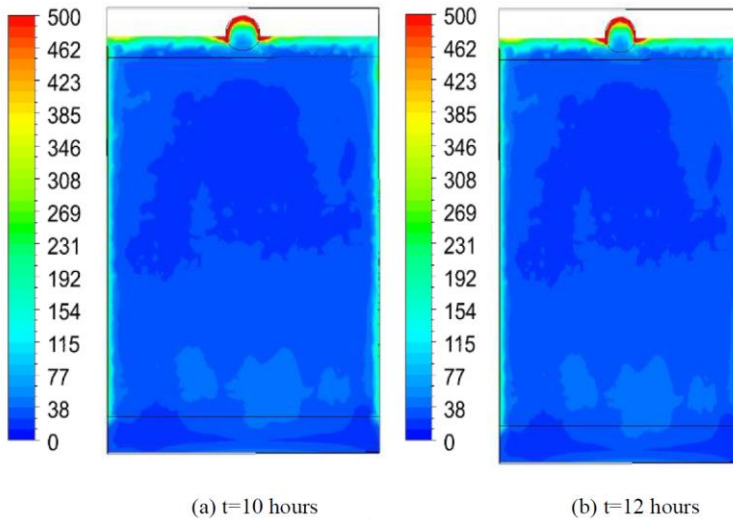

Figure 23. (Continued onto next page).

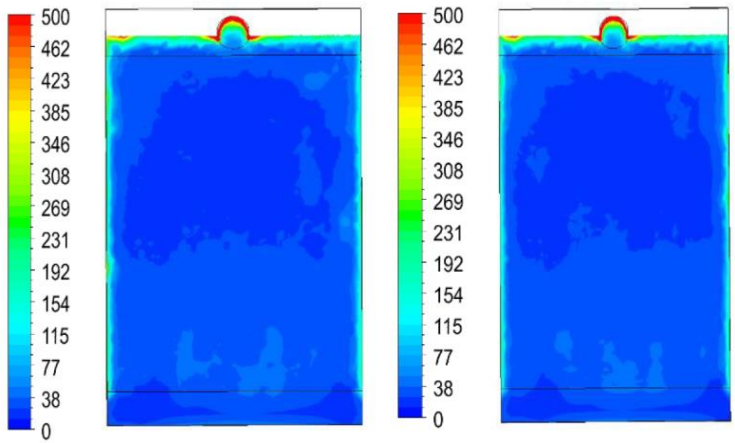

Figure 23. Distribution of the turbulent eddy frequency in the second passage.

4.7. Turbulent Viscosity

Figures 24, 25 and 26 show the distribution of the turbulent viscosity in the different longitudinal and transverse planes for the first and second passages of the solar air heater supplying the box prototype at t=10 hours, t=12 hours, t=14 hours and t=16 hours. According to these results, it is clear that the turbulent viscosity presents the same distribution at the different considered instances. For example, at t=12 hours, a wake zone characteristic of the maximum value of the turbulent viscosity has been observed around the collector inlet of the solar air heater. This wake is expanded in the first passage near the absorber side. In these conditions, the maximum value of the turbulent viscosity is equal to μ_t=0.002 kg.m^{-1}.s^{-1}. Away from this area, the turbulent viscosity presents a very weak value. The same fact has been observed in the second passage, where the maximum value is equal to μ_t=0.001 kg.m^{-1}.s^{-1} in the first mid-plane. In the absorber, the turbulent viscosity reaches a null value. At the exit of the second passage, a slight increase of the turbulent viscosity until μ_t=0.002 kg.m^{-1}.s^{-1} has been observed in the first part of the pipe connecting the solar air heater with the box prototype. In the remainder of the pipe, the turbulent viscosity decreases and presents very low values. In the hole inlet of the box prototype, the low values of the turbulent viscosity continue to appear in the first part of the discharge area. In the second part, a slight increase of the turbulent viscosity has been observed on the side of the

reverse wall. In the rest of the domain of the box prototype, a wake zone characteristic of the maximum value of the turbulent viscosity, equal to μ_t=0.007 kg.m^{-1}.s^{-1}, has been created. This fact can be explained by the recirculation zone appeared in the whole area of the box prototype. Indeed, a rapid expansion of the turbulent viscosity until μ_t=0.012 kg.m^{-1}.s^{-1} has been observed in the hole outlet of the box prototype. By comparing the turbulent viscosity for the different instances, it is clear that the maximum value of the turbulent viscosity is obtained at t=12 hours and it is equal to μ_t=0.0131 kg.m^{-1}.s^{-1}. For the other instances, the turbulent viscosity decreases and the minimum values are obtained at t=16 hours. At this instance, the maximum value of the turbulent viscosity is equal to μ_t=0.012 kg.m^{-1}.s^{-1}.

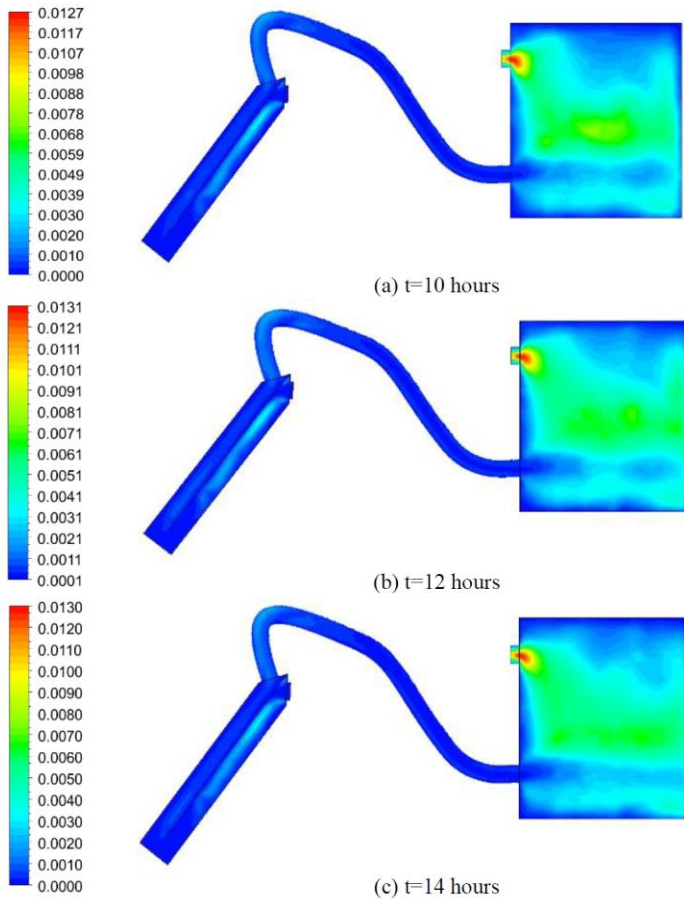

Figure 24. (Continued onto next page).

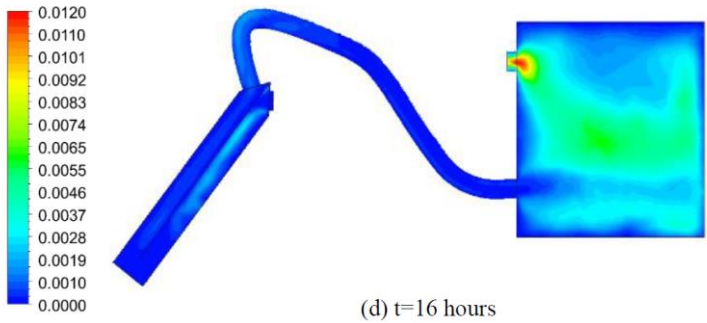

Figure 24. Distribution of the turbulent viscosity in the longitudinal plane.

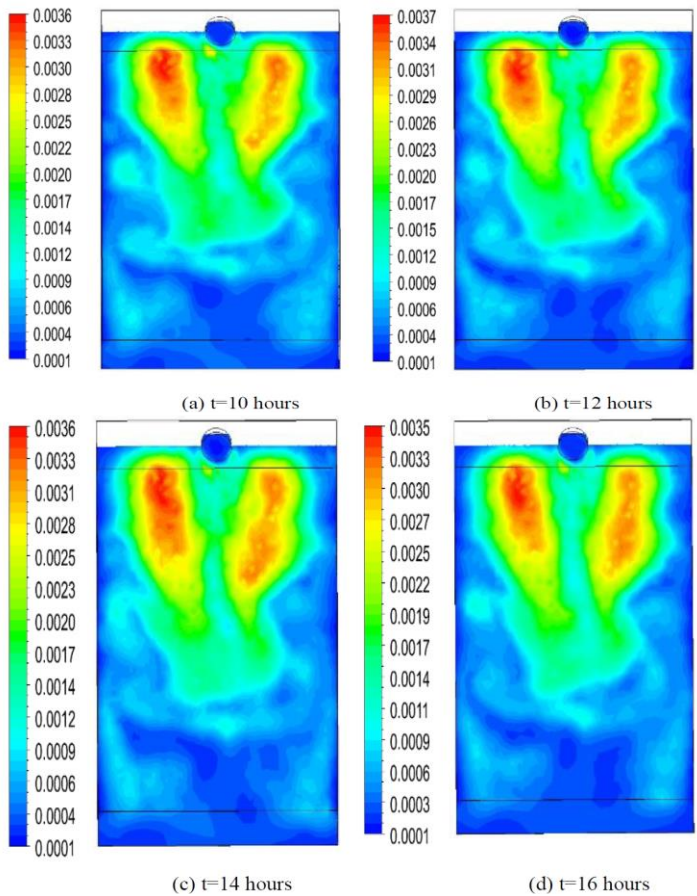

Figure 25. Distribution of the turbulent viscosity in the second passage.

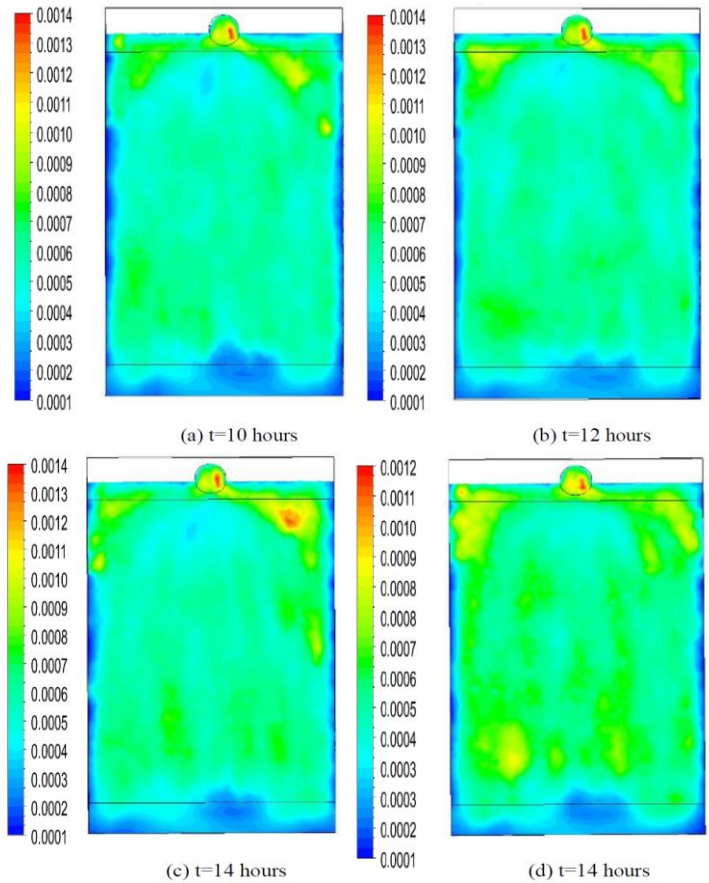

Figure 26. Distribution of the turbulent viscosity in the second passage.

5. Comparison with Experimental Results

Figures 27 and 28 compare the numerical results of the temperature and velocity profiles in the second channel superposed with our experimental results in a fan delivery mode side the insulation. Different instances equal to t=8 hours, t=10 hours, t=12 hours, t=14 hours, t=16 hours and t=18 hours have been considered. According to these results, a similar appearance between the curves has been observed for the magnitude velocity with a small difference between the calculated values. However, this difference is more clear for the temperature profiles. In fact, in these conditions, the maximum values of the

temperature are obtained at t=12 hours. By comparing these obtained results, it has been observed that the temperature values decrease slightly at t=14 hours. However, the minimum values of the temperature is obtained at t=18 hours. For the others instances t=10 hours, t=16 hours and t=8 hours, the temperature values decrease immensely. The comparison of the numerical results with our experimental data picked up on 28 August 2017 at t=12 hours, presents a good agreement with a gap equal to 6%. These results confirm the validity of our numerical method.

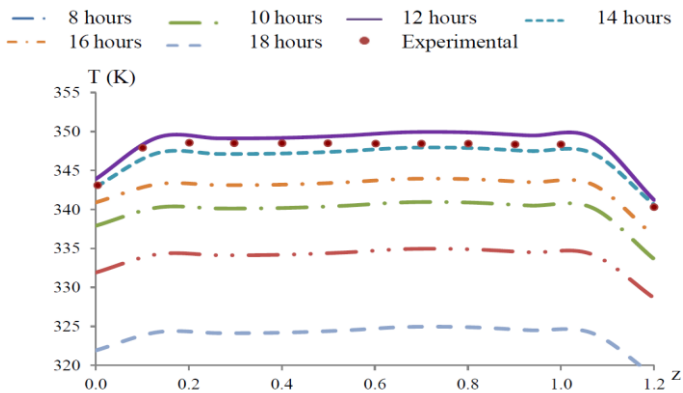

Figure 27. Profiles of the temperature in the second channel.

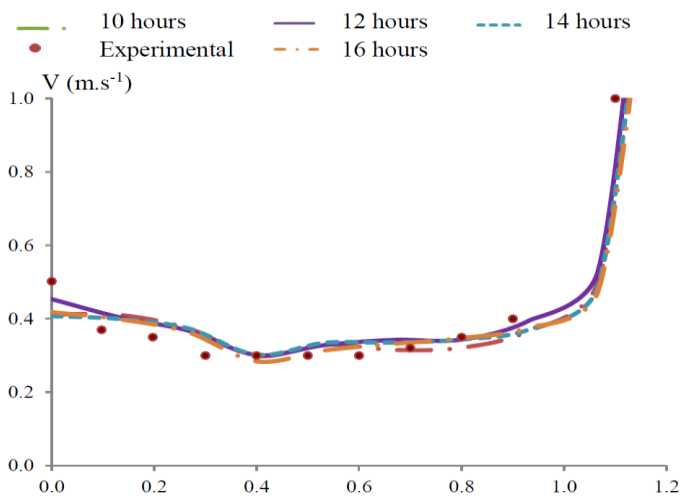

Figure 28. Profile of the magnitude velocity in the second channel.

6. Energy Efficiency

Figure 29 presents the profile of the energy efficiency which confirms the results obtained over the time. In fact, at the beginning of the day, the energy efficiency has very low values. With the increase of the temperature through the day, there is a gradual increase of the energy efficiency until t=12 hours, with a value equal to η= 31.8%. In the first half day, it has been noted that the increase of the energy efficiency is more important after t=10 hours. Afternoon, the energy efficiency starts to decrease with a constant slope. At t=18 hours, the energy efficiency is very low and it is equal to η= 24.8%.

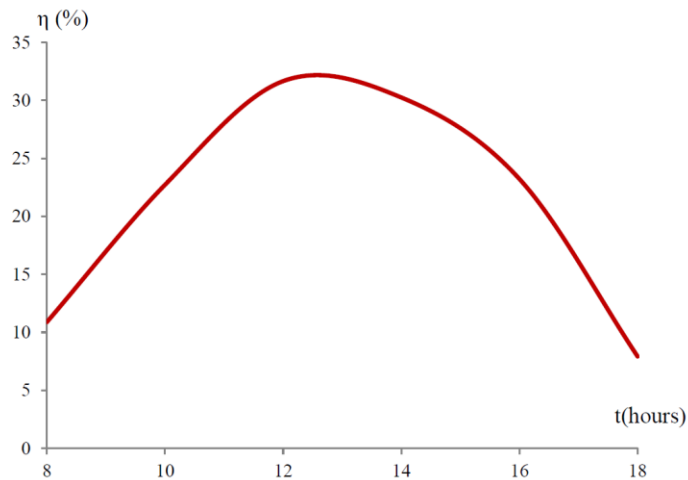

Figure 29. Energy efficiency profile.

Conclusion

Since the solar air heater is not very commonly used in the domestic and industrial applications, we are interested on the design and the realization of a new solar air heater test bench to investigate the efficiency of the solar system. The considered test bench consists of two passages solar air heater separated by an absorber and powered by a fan working in a delivery mode and placed in the inlet, side the insulation. On the glass side, it is connected to the box prototype through a pipe. On this system, a glass is hanging on the front side and an absorber is inserted inside. The hot air flow is routed towards the box

prototype. Two circular holes, are located in the same face of the box prototype. The inlet hole allows the hot air supply. However, the outlet hole allows its escape into the ambient environment. Indeed, we have developed numerical simulations to study the turbulent flow in the considered test bench over the day. In these conditions, it has been observed a decrease in the flow and an appearance of the recalculation zones in the first passage. This phenomenon is more prominent during the transition of the flow to the second passage. However, the flow becomes uniform until the exit of the solar air heater. Via the pipe separating the solar air heater from the box prototype, a discharge area appears in the hole inlet and invaded the reverse wall. By comparing the local characteristics for the different instances, a similar appearance has been observed with a maximum value at t=12 hours. For the magnitude velocity, a small difference between the calculated values has been noted. However, this difference is more clear for the temperature distribution and the turbulent characteristics. For the energy efficiency, it presents very low values at the beginning of the day. With the increase of the temperature through the day, there is a gradual increase of the energy efficiency until t=12 hours, with a value equal to η= 31,8%. This technology will be very useful since it can provide sustainable energy and substitute the expensive traditional technologies.

References

[1] Bakri, B., H. Benguesmia, A. Ketata, S. Driss, Z. Driss, Prediction of the unsteady turbulent flow in a solar air heater test bench, *Modelling, Measurement and Control B*, Vol. 89(1-4), 2020, 7-13.

[2] Ayadi, A., Z. Driss, A. Bouabidi, H. Nasraoui, M. Bsisa, M. S. Abid, A computational and an experimental study on the effect of the chimney height on the thermal characteristics of a solar chimney power plant, *Journal of Process Mechanical Engineering*, 231 (2017) 1-14.

[3] Driss, S., Z. Driss, I. Kammoun, Numerical simulation and wind tunnel experiments on wind-induced natural ventilation in isolated building with patio, *Energy*, 90 (2015) 917-925.

[4] Benguesmia, H., B. Bakri, Z. Driss, Effect of the turbulence model on the heat ventilation analysis in a box prototype, *Diagnostyka*, 21(3) (2020), 55-66.

[5] Bakri, B., S. Driss, A. Ketata, Z. Driss, H. Benguesmia, F. Hamrit, Study of the Heat Ventilation in a Box Prototype With the k-ω Turbulence Model, *Transylvanian Review Journal*, Vol XXXVI (30) (2018)7989-8000.

[6] Bakri, B., O. Eleuch, A. Ketata, S. Driss, Z. Driss, H. Benguesmia, Study of the turbulent flow in a newly solar air heater test bench with natural and forced convection modes, *Energy*, 161(2018)1028-1041.

[7] Bakri, B., A. Ketata, S. Driss, H. Benguesmia, Z. Driss, F. Hamrit, Unsteady investigation of the heat ventilation in a box prototype, *International Journal of Thermal Sciences*, 135 (2019)285–297.

[8] Bakri, B., S. Driss, A. Ketata, H. Benguesmia, F. Hamrit, Z. Driss, Study of the meshing effect on the turbulent flow in a building system with a k-ω turbulence model. *International Conference on Mechanics and Energy (ICME'2016)*, December 22-24 2016, Hammamet, Tunisia.

[9] Bakri, B., A. Ketata, S. Driss, H. Benguesmia, F. Hamrit, Z. Driss, Effect of the turbulence model on the aerodynamic structure to evaluate the thermal comfort in a building system, *International Conference on Mechanics and Energy (ICME'2016)*, December 22-24 2016, Hammamet, Tunisia.

[10] Bakri, B., A. Ketata, S. Driss, Z. Driss, H. Benguesmia, F. Hamrit, Unsteady simulation of the aerodynamic structure in a heated box prototype, *International Conference on Mechanics and Energy (ICME'2017)*, December 18-20 2017, Sousse, Tunisia.

[11] Bakri, B., S. Driss, A. Ketata, Z. Driss, H. Benguesmia, F. Hamrit, Study of the turbulent flow in a box prototype with the k-ω turbulence model, *Congrès Algérien de Mécanique, (CAM2017-289)*, 26-30 Novembre, Constantine-Algérie.

[12] Bakri, B., H. Benguesmia, A. Ketata, S. Driss, Z. Driss, F. Hamrit, Study of the Natural Convection Flow in a Solar Air Heater Test Bench, *International Conference on Mechanics and Energy (ICME'2018)*, December 20-22 2018, Hammamet, Tunisia.

[13] Bakri, B., H. Benguesmia, A. Ketata, H. Nasraoui, Z. Driss, Performance evaluation of the natural-convection of a solar air-heater with a plate absorber, *International Conference on Mechanics and Energy (ICME'2018)*, December 19-21 2019, Monastir, Tunisia.

[14] Bakri, B., H. Benguesmia, Study of the forced convective heat transfer in a solar air heater, *The First International Conference on Materials, Energy and Environment (MEE'2020, N°: EO05)*, January 20-21, 2020, El Oued University, Algeria.

[15] Bakri, B., H. Benguesmia, A. Ketata, S. Driss, Z. Driss, A comparative study of the turbulence models on the heat ventilation in a box prototype, *1ère Conférence National sur: la Transition Énergétique en Algérie Conférence (CNTEA1-2020)*, Mars 8-9, 2020, M'sila, Algeria.

[16] Bakri, B., H. Benguesmia, A. Ketata, S. Driss, Z. Driss, Choice of the appropriate turbulence model for modeling the air flow inside a room, *1ère Conférence National sur: la Transition Énergétique en Algérie Conférence (CNTEA1-2020)*, Mars 8-9, 2020, M'sila, Algeria.

[17] Bakri, B., H. Benguesmia, A. Ketata, S. Driss, Z. Driss, CFD based performance analysis of a solar air heater test bench with unsteady turbulent flow, 9ème *Journées des sciences de l'ingénieur JSI'2020,* September 25-27, 2020, Sfax, Tunisia.

[18] Driss, Z., O. Mlayeh, D. Driss, M. Maaloul, M.S. Abid, Numerical simulation and experimental validation of the turbulent flow around a small incurved Savonius wind rotor. *Energy*, 74 (2014) 506-517.

[19] Driss, Z., G. Bouzgarrou, W. Chtourou, H. Kchaou, M.S. Abid. Computational studies of the pitched blade turbines design effect on the stirred tank flow characteristics. *European Journal of Mechanics B/Fluids*, 29, 2010, 236-245.

[20] Driss, Z., O. Mlayah, S. Driss, M. Maaloul, M.S. Abid, Study of the incidence angle effect on the aerodynamic structure characteristics of an incurved Savonius wind rotor placed in a wind tunnel, *Energy*, 113 (2016) 894-908.

[21] Driss, Z., O. Mlayah, S. Driss, D. Driss, M. Maaloul, M.S. Abid, Study of the bucket design effect on the turbulent flow around unconventional Savonius wind rotors, *Energy*, 89 (2015) 708-729.

[22] Yang, M., X. Yang, X. Li, Z.Wang, P. Wang, Design and optimization of a solar air heater with offset strip fin absorber plate, *Applied Energy*, 113 (2014) 1349-1362.

[23] Altaa, D., E. Bilgilib, C.Ertekina, O. Yaldiza, Experimental investigation of three different solar air heaters: Energy and exergy analyses, *Applied Energy*, Volume 87 (2010) 2953-2973.

[24] Zukowski, M., Experimental investigations of thermal and flow characteristics of a novel microjetair solar heater, *Applied Energy*, 142 (2015) 10-20.

[25] El-Sebaii, A. A., S. Aboul-Enein, M. R. I. Ramadan, S. M. Shalaby, B. M. Moharram, Thermal performance investigation of double pass-finned plate solar airheater, *Applied Energy*, 88 (2011) 1727–1739.

[26] Wazed, M. A., Y. Nukman, M. T. Islam, Design fabrication of a cost effective solar air heater for Bangladesh, *Applied Energy*, 87 (2010) 3030–3036.

[27] Esen, H., Experimental energy and exergy analysis of a double-flow solar airheater having different obstacles on absorber plates, *Building and Environment*, 43 (2008) 1046-1054.